Mapping land degradation risk due to land susceptibility to dust emission and water erosion

Mahdi Boroughani[1*], Fahimeh Mirchooli[1, 2], Mojtaba Hadavifar[3], Stephanie Fiedler[4]

[1]Research Center for Geoscience and Social Studies, Hakim Sabzevari University, Sabzevar, Iran.

[2]Sari agricultural Science and Natural Resources University, Sari, Iran

[3]Environmental Sciences Department, Hakim Sabzevari University, Sabzevar, Iran

[4]University of Cologne, Institute of Geophysics and Meteorology, Cologne, Germany

(Corresponding Author: m.boroughani@hsu.ac.ir)

Abstract

Land degradation is a cause of many social, economic, and environmental problems. Therefore identification and monitoring of high-risk areas for land degradation are necessary. Despite the importance of land degradation due to wind and water erosion, the topic receives often relatively little attention. The present study aims to create a land degradation map in terms of soil erosion caused by wind and water erosion of semi-dry land. We focus on the Lut watershed in Iran encompassing the Lut Desert that is influenced by both monsoon rainfalls and dust storms. Dust sources are identified using MODIS satellite images with the help of four different indices to quantify uncertainty. The dust source maps are assessed with three machine learning algorithms encompassing artificial neural network (ANN), random forest (RF), and flexible discriminant analysis (FDA) to map dust sources paired with soil erosion susceptibility due to water. We assess the accuracy of the maps from the machine learning results with the metric Area Under the Curve (AUC) of the Receiver Operating Characteristic (ROC). The water and aeolian soil erosion maps are used to identify different classes of land degradation risks. The results show that 43% of the watershed is prone to land degradation in terms of both aeolian and water erosion. Most regions (45%) have a risk of water erosion and some regions (7%) a risk of aeolian erosion. Only a small fraction (4%) of the total area of the region had a low to very low susceptibility for land degradation. The results of this study underline the risk of land degradation for in an inhabited region in Iran. Future work should focus on land degradation associated with soil erosion from water and storms in larger regions to evaluate the risks also elsewhere.

Key words: Desertification, Desert-dust sources, Risk susceptibility, Water-induced soil erosion,

Introduction

Land degradation is one of the most pressing environmental issues around the globe. Several aspects of this issue have been recognized by the United Nations Convention (Gholami et al. 2019a). Land degradation can be driven by both water and wind, of which the former can have a stronger impact on soil erosion in a short time (Gia et al. 2018). A total of 30% of global land area and three billion people are affected by land degradation (Wieland et al., 2019). In Iran, it is estimated that land and water degradation cost about US $12.8 billion per year which is four percent of the total Gross Domestic Product (GDP) (Emadodin et al. 2012). Therefore, spatial mapping of risks of land degradation is necessary which can provide a basis to support managers and policymakers in risk mitigation and adaptation to aeolian and water erosion.

Land degradation driven by aeolian erosion is a known problem (Shi et al. 2004). Dust storms, which are a natural hazard, are associated with soil erosion. This phenomenon has detrimental impacts on the Earth system, e.g., for food security (Boroughani et al. 2022), water supply (Duniway et al., 2019), human health (Moridnejad et al., 2015), geochemical conditions (Gholami et al., 2020b), and the Earth's carbon cycle (Gherboudj et al., 2017). Identifying dust sources as potential areas of dust emission is therefore necessary for developing a better understanding of land degradation. Spatial mapping of dust source susceptibility areas (DSSAs) is a crucial step for erosion mitigation and watershed management.

In addition to soil erosion by wind, water-driven soil erosion is a known mechanism for soil degradation. This kind of soil erosion is a known environmental threat and can influence both terrestrial and aquatic systems (Halecki et al. 2018, Sun et al. 2014). Therefore, knowing the spatial distribution of water-induced soil erosion susceptibility areas (SESA) is also necessary.

Different approaches for identifying DSSAs exist, e.g., using meteorological data (Yang et al. 2019), numerical modeling (Péré et al. 2018), and remote sensing (Jafari et al. 2021). Remote sensing can provide worldwide information on aerosol properties (Park et al. 2014). The present study uses Moderate Resolution Imaging Spectroradiometer MODIS satellite images in combination with machine learning to

detect dust aerosols and map its susceptibility over the Lut Desert. Moreover, several numerical models exist for predictions and risk evaluations of water-induced soil erosion (Chicas et al., 2016, Gao et al., 2017, Anache et al., 2018, Gia et al., 2018, Halecki et al., 2018), but none used machine learning to combine different observational data sets for assessing soil erosion. Machine learning has emerged as a subfield of data science and helps to better understand environmental problems (Gholami et al. 2019b). It can integrate data from different sources to create forecasts and discover patterns (Gholami et al. 2020a). In environmental sciences, algorithms such as support vector machine, random forest (RF), artificial neural networks (ANN), and multivariate adaptive regression spline have been applied, e.g., for groundwater (Lee et al. 2017), gully erosion (Zabihi et al. 2018), sediment contamination (Mirchooli et al. 2019), dust sources (Boroughani et al. 2020), landslides (Youssef and Pourghasemi 2021), floods (Tehrany et al. 2014), and trace elements (Derakhshan-Babaei et al. 2022).

However land susceptibility to soil erosion and dust emsission has been assessed in different and separate studies, it has attracted less attention to investigate both of them in the same study. So, the novelty of this study lies in constructing an integrated framework based on field survey, different environmental factors, and machine learning algorithms to assess both of water erosion and dust emission.

This research is conducted to test some hypotheses including (1) the central and western parts of the watershed are the highest susceptible areas to water erosion and aerosol emission, respectively (2) NADI and land use are the most important factors for water erosion and aolian emission and (3) Central areas are the most prone parts of the watershed to these phonemona. Correspondigly, the aims of the current study are (1) to assess the spatially resolved contribution of soil erosion by water and wind using three machine learning algorithms, (2) determine the most important factor influencing water and dust emission susceptibility and (3) to combine the findings into spatially resolved information on risks for land degradation and recognize the hotspot area in terms of water erosion and dust emission.

2. Data and methods

The focus of this study is on the Lut watershed situated in the east and southeast of Iran covering an area of 206242 km^2 (28º 10' to 32º 30' N latitude and 55º 45' to 61º 15' E longitude) and is marked in Fig. 1. This watershed include a great diversity of

topographic charactristics, with an elevation ranging from 124 to 4269m, and slope ranging from 0 to 28.04 degree. In this region, southwest and northeast aspects have the most frequencies (34% of the area). This watershed covers some parts of the South Khorasan, Yazd, Kerman, and Sistan-Baluchestan Provinces of Iran. In addition, several important cities and towns such as Birjand, Tabas, Bam located in the watershed. Aridisols is the dominant soil order of the watershed in which it constitutes 40.1% of this region. The studywatershed includes the largest desert of the country, the Lut Desert. The region contributes to the increasing dust concentration in southwest Asia (Ebrahimi-khusfi et al. 2021). This area is chosen to develop and test the methods based on regional data on erosion observations with examples shown in Fig. 1a-d. It underlines the impacts of land degradation that goes well beyond impacts on the natural environment.

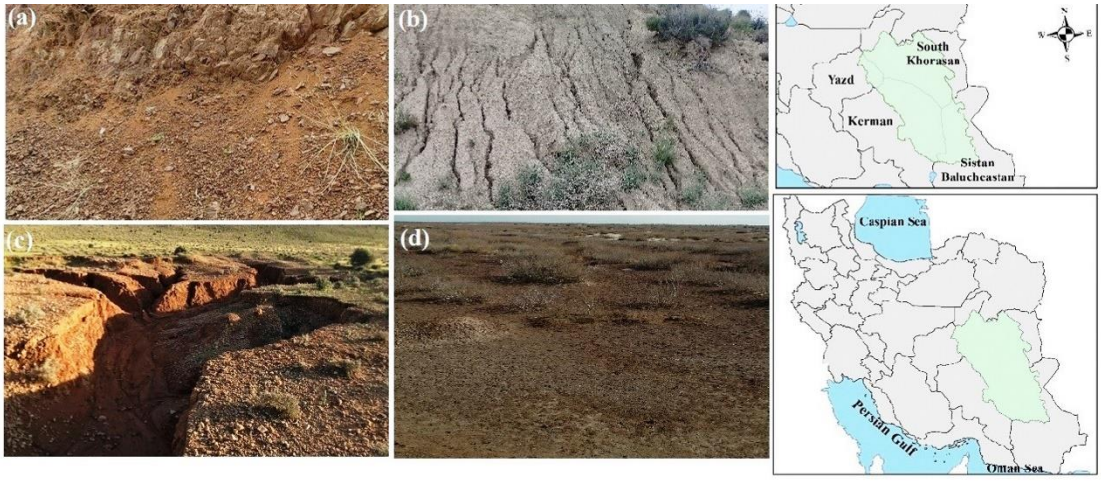

Fig.1 Geographical location of the study watershed. Green shading marks the Lut watershed. The Lut Desert is located in the centre of the watershed. Settlements are primarily situated in the northern and south-western parts. Example of soil erosion in the watershed are sheet erosion (a), rill erosion (b), gully erosion (c), and wind erosion (d).

2. 1. Land degradation mapping

Our land degradation zonation consists of three main processing steps, graphically depicted in Fig. 2. At first, spatial mapping of water erosion is conducted (section 2.1.1). In the second step, spatial mapping of dust source susceptibility is carried out with machine learning methods (section 2.1.2). In the last step, the patterns of water erosion and dust source susceptibility are combined to identify risk areas of land degradation (section 2.2.3).

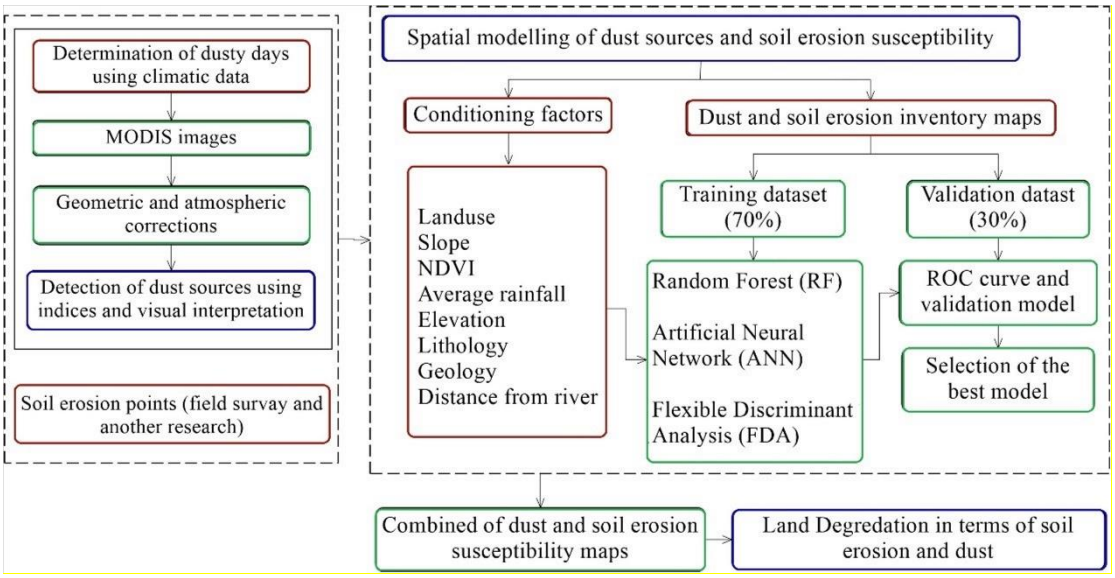

Fig.2 Flowchart of inputs (red boxes), data processing (green boxes), and outputs (blue boxes) in the present study

2.1.1 water erosion map

Quantifying the erosion susceptibility of an area requires to determine a spatial distribution of observed water-induced soil erosion that can have different characteristics, e.g., gully erosion, rill erosion, and surface erosion. That information is extracted from data collected during an own field survey paired with previous research (Shit et al. 2020). In the previous research, a combination of consulting with provincial experts, satellite images, recent aerial photos, and field survey were applied to identify soil erosion. The aim of the field survey for the present study was to identify regions where sheet, rill, and gully erosion took place. This field survey was carried out in accessible parts of the watershed in April 2020. These accessible parts are mostly distributed around the cities (such as Bam, Ravar, Shahdad, Baravar, Birjand, Tabas, etc) with proper road access located in the watershed. The data set contains the type of water-induced soil erosion along with the geographical location using a Global Positioning System (GPS). A selection of the identified water soil erosions in the study region is shown in Fig. 1.

We translated the observations of the field survey into maps of non-degraded and degraded areas. These areas were plotted in an inventory map and prepared for further analysis, although not all desert areas are fully covered by the survey.

2.1.2 Dust aerosol map

The large desert area to be covered is a motivation for the use of satellite data for estimating dust sources. We used MODIS images from the Terra (morning) and Aqua (afternoon) satellites (Vickery and Eckardt, 2013) to identify dust aerosols. We define dusty days, when the horizontal visibility is less than 2000 m for at least one hour during the day based on available weather stations in Iran (Vickery and Eckardt, 2013; Boroughani et al., 2021). According to the mentioned condition, more than 500 dusty days were identified during 2010–2021 distributed over the stations in Birjand, Zahedan, Kerman, Bam, Doostabad, Bisheh, Rafsanjan and Mighan. We pair the station observations with satellite data to estimate the spatial extent of the dust aerosol plumes. Due to the overpass of the Terra and Aqua satellites once per day, we acquired 28 satellite images from the MODIS sensor that during times when the weather stations had documented dusty conditions in the ten-year period. For identifying pixels with dust aerosols in these images, we calculate four different dust indices (BTD2931, BTD3132, NDDI and D) for dust aerosol identification (Boroughani et al., 2020, 2021 Hahnenberger and Nicoll, 2014).

$$B(T,\lambda) = \frac{2hc^2}{\lambda^5 \frac{hc}{(e\lambda kt-1)}} \quad (1)$$

where B(T, λ) represents the Planck equation at λ (μm), T is the BT (K), h is the Planck's constant (6.626×10^{-34} m^2kgs^{-1}), k is the Boltzmann's constant (1.38×10^{-23})[5], c is the speed of light (2.99×10^{8} ms^{-1}), and T is the temperature (Hao et al., 2007)

$$T = \frac{hc}{\lambda k ln(1+\frac{2hc^2}{L\lambda^5})} \quad (2)$$

Using Planck's equation, the value of the temperature can be derived, where L is the amount of radiance in the images (in $Wm^{-2}sr^{-1}\mu m^{-1}$).

$$NDDI = (p_{2.13} - p_{0.469})/(p_{2.13} + p_{0.469})$$

(3)

where $\square_{2.13}$ and $\square_{0.469}$ depict the reflectance value at the top-of-atmosphere at 2.13 and 0.469 μm, respectively (Qu et al., 2006)

$$D = exp\{-[rr \times a + (BTD - b)]\} \quad (4)$$

where rr shows the reflectance proportion among wavelengths of 0.54 μm and 0.86 μm and BTD is the difference among the bands 11 and 12 μm; a and b are constants taken during the initial calibration (Eq. 1). (Qu et al., 2006; Miller, 2003; Hao et al., 2007; Boroughani et al., 2020, 2021).

We compute false color maps using four combinations of channels (1: NDDI, B4, B3; 2: D, BTD2931, NDDI; 3: D, BTD3132, NDDI; and 4: BTD2931, B4, B3) in ENVI software. We choose these four different indices for cross-validating the presence of dust aerosols. With each of these methods we see dust aerosol in different color and qualities in the MODIS images over 28 days. After combining the four methods in the software ENVI, we choose the method that shows the dust plume in the MODIS image more clearly as the best method (Boroughani et al., 2020, 2022). This method is based on a cone of dust diffusion seen in the processed MODIS images, where the apex denotes the dust's source (Lee et al., 2009; Walker et al., 2009). Ultimately, the inventory map of the dust aerosols in the Lut watershed was created.

2.2. Identification of key factors controlling for aeolian and water erosion

To develop DSSA and SESA, the identification and selection of appropriate dust sources and soil erosion effective factors are necessary. The main factors affecting DSSA and SESA were selected and constructed based on literature, available data and geographical maps (Torabi et al., 2021; Zabihi et al., 2018; Boroughani et al., 2020; Gholami et al., 2020a). The considered factors in this study included: elevation, land use, slope of terrain, lithology, annual rainfall, distance from rivers, and distance from roads, the Topographic Wetness Index (TWI), and Normalized Difference Vegetation Index (NDVI). Various sources were used to gather data for these factors, introduced in the following in more detail. All collected data were mapped to a horizontal grid of 1km resolution.

The shuttle radar topography mission (SRTM) images were used to create the digital elevation model (DEM, , Fig 3c) (Ghorbanzadeh et al., 2018). The lowest and highest elevation of the study area is 124 m in the centre of the desert and 3966 m at the western and eastern margins of the study watershed, respectively (Fig. 3c). Vegetation cover considerably supports soil conservation. Areas with low vegetation cover would be more sensitive to both erosion by water and wind (Arabameri et al., 2019a; Gholami et al. 2019b). Therefore, we use the Normalized Difference Vegetation Index (NDVI) to

assess the vegetation cover in the study area from MODIS images following (Arabameri et al., 2019a; Boroughani et al., 2020):

$$NDVI=\frac{NIR+R}{NIR-R}$$

Where R is the red (0.620-0.670 µm) and NIR is near-infrared bands (0.841-0.876 µm) (Fig. 3d).

Annual rainfall (Fig. 3e) was obtained from Iran Meteorological Organization for the period of 2000-2021. Mean annual rainfall was calculated using 40 different meteorological stations located within or close to the watershed (Fig.3e). The inverse distance weighting (IDW) interpolation method was applied to integrate rainfall over the study area in the ArcGIS environment (Gholami et al., 2020a). Topographic Wetness Index (TWI), which indicates the spatial distribution of areas of potential soil saturation, is an effective factor to indicate water erosion including landslides and also flooding (Arabameri et al., 2019b). TWI which determines the dry and wet zones calculated as (Beven and Kirkby 1979):

$$TWI = ln(\frac{\alpha}{tan\beta})$$

where α is the cumulative up-slope area from a point (per unit contour length) and β is the slope angle at that point. This index was calculated in the SAGA-GIS environment and classified into four groups viz. 14-17, 17-19, 17-21, 21-24 (Fig. 3f). The aspect map was also generated using DEM and grouped into ten classes (Fig. 3 g). Distance from road is an indicator of infrastructure development which influences soil erosion and land degradation (Torabi et al., 2021). This factor is shown in five classes in Fig. 3 h. Distance from river is one of the most effective factors on water-caused erosion (Amiri et al., 2019) which is classified into six groups (Fig. 3i).

The slope map (%) was created using a Digital Elevation Map (DEM, Fig. j) and classified into five groups including 0-3%, 3-6%, 6-12%, 12-21%, and 21-54%. The lithology map indicates eleven different soil classes in the study area (Fig. 3k).

Land use and soil maps were obtained from base maps developed by the Iranian Forest, Rangeland, and Watershed Management Organization (https://frw.ir/). In the study region, there are fourteen land-use classes including wetlands, rangelands of three states (poor, medium, and rich), dry farming, agricultural lands, urban area, fallow land, rock-covered land, wetland, saltland, woodland, bare surfaces, and sand dunes (Fig. 3m). A large percentage (83%) of the watershed area is covered by bare land, poor rangeland,

and sand dunes. All three land use classes are prone to wind erosion due to sparse or no vegetation.

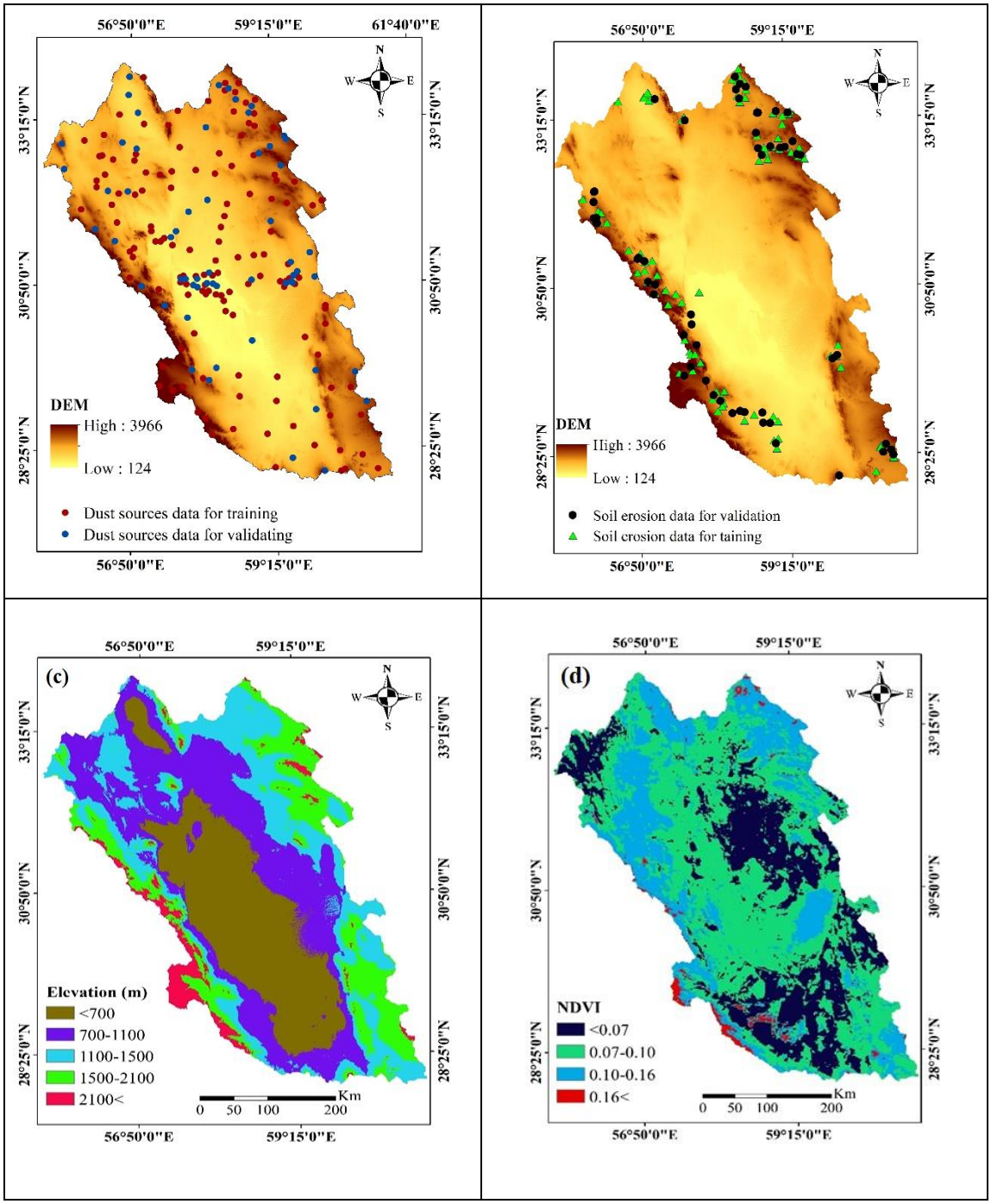

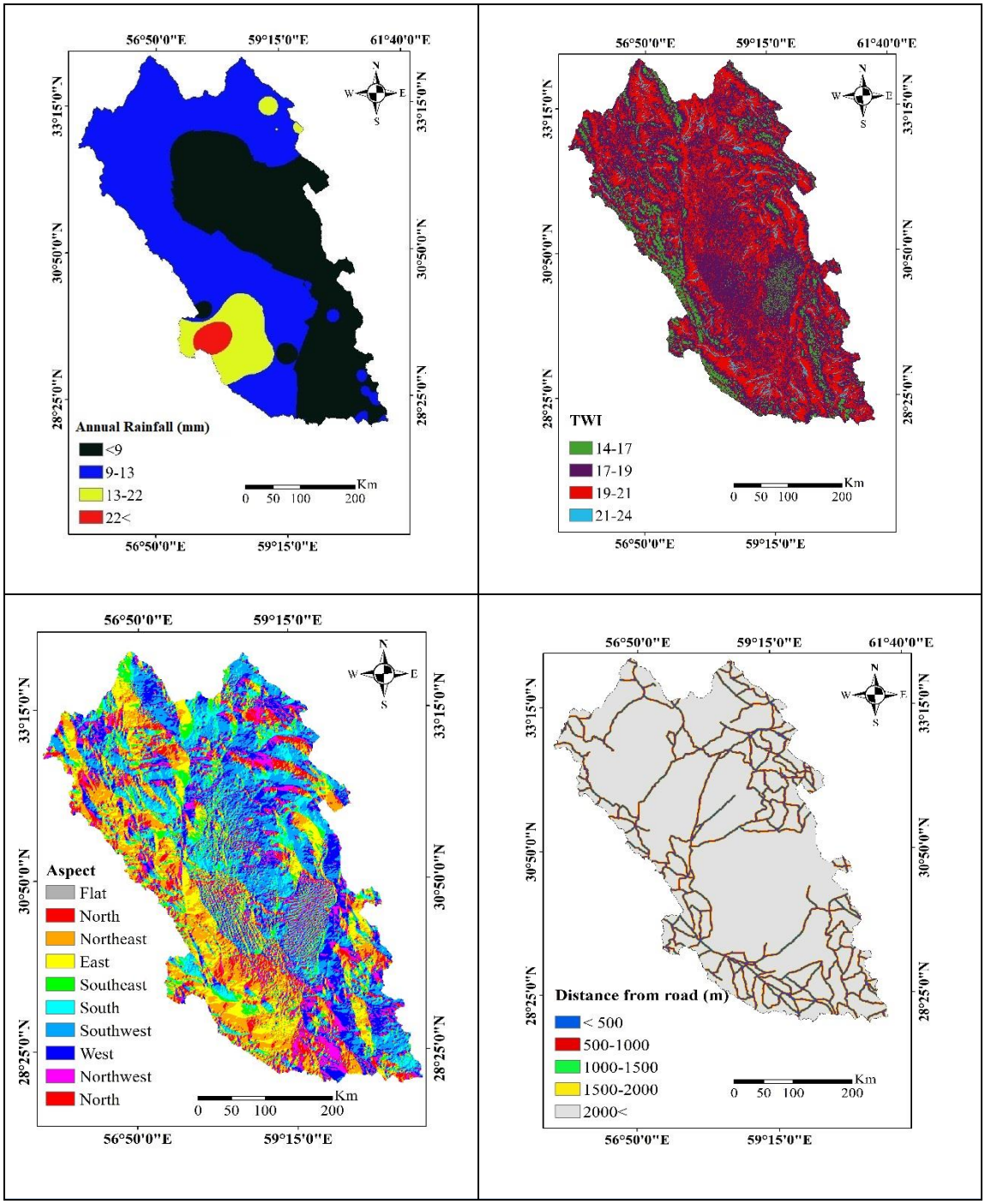
56°50'0"E
59°15'0"E
61°40'0"E
33°15'0"N
30°50'0"N
28°25'0"N
N
W
E
S
Annual Rainfall (mm)
<9
9-13
13-22
22<
Km
0 50 100 200
TWI
14-17
17-19
19-21
21-24
Aspect
Flat
North
Northeast
East
Southeast
South
Southwest
West
Northwest
North
Distance from road (m)
< 500
500-1000
1000-1500
1500-2000
2000<

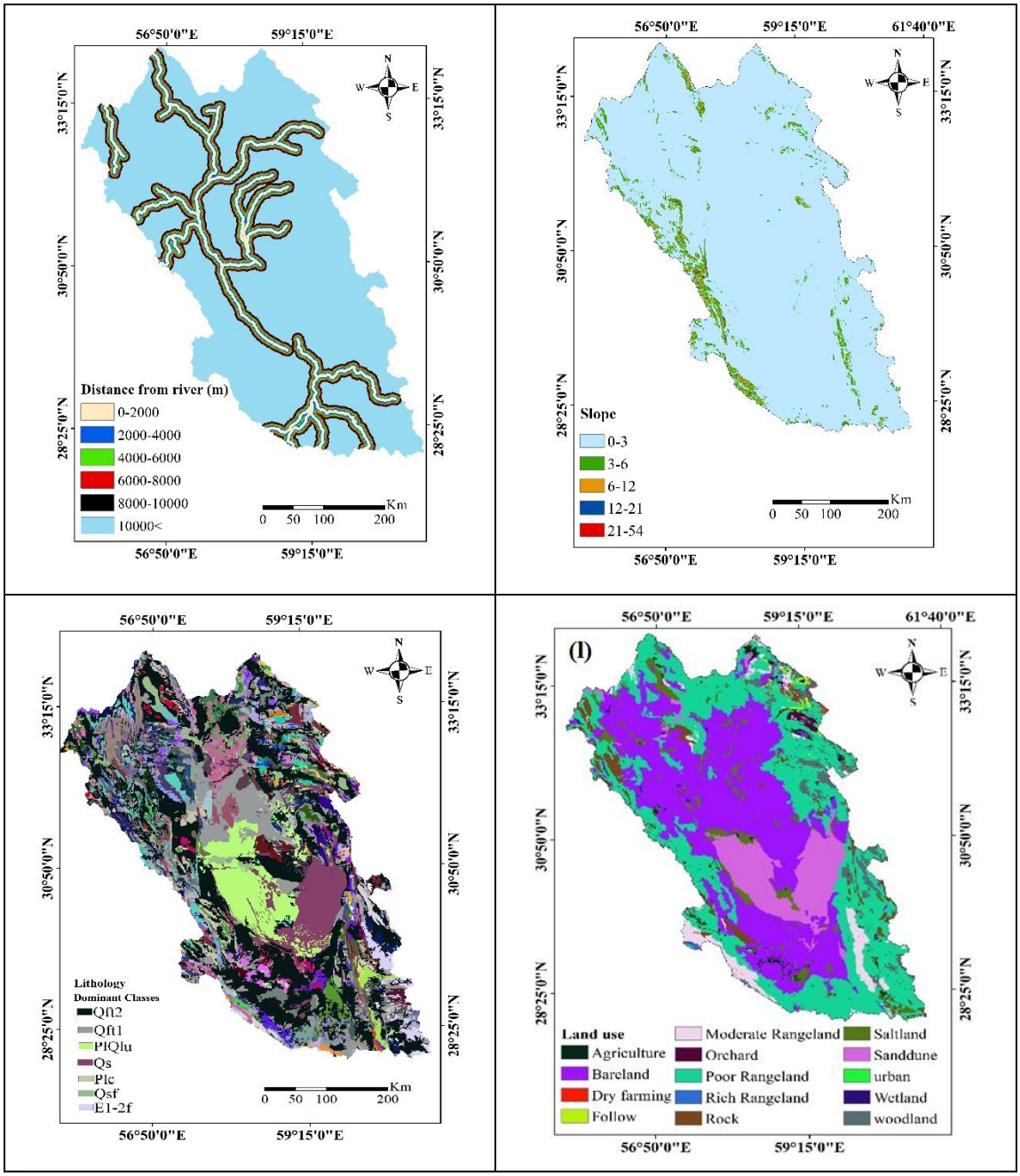

Fig.3 Location of dust observation points for training and validation (a), water-induced soil erosion points for training and validation (b), and the conditional factors (Elevation (c), NDVI (d), Rainfall (e), TWI (f), Aspect (g), Distance from road (h), Distance from river (i), Slope (j), Lithology (k), Land use (l)) in the watershed.

2.4. Spatial mapping of DSSA and SESA using machine learning algorithms

We combine the two susceptibility maps for DSSA and SESA to create the land degradation hazard map with regards to water- and wind-induced soil erosion. For both types of soil erosion, three machine learning models were constructed and applied. The land degradation susceptibility map was then created by synthesizing the results for

both soil erosion types in an ArcGIS 10.5 environment, and the land degradation susceptibility was ultimately evaluated with four classes.

A wide range of machine learning algorithms has been applied for spatial mapping of environmental phenomena in the past. The effective factors described in Section 2.2 and the inventory maps of water and wind erosion were used as the input of the machine learning algorithms. In the present study, the algorithms of random forest (RF), artificial neural network (ANN), and flexible discriminate analyses (FDA) were used to produce DSSA and SESA maps. We choose three different algorithms to test the dependency of the results on the method as a measure of uncertainty. The three algorithms are described in more detail in the following.

2.4.1 Random forest (RF)

Random forest developed by Breiman (2001) is a machine learning algorithm for non-parametric multivariate classification. RF builds multiple trees using a random selection of the training dataset. The data not included are called out-of- bag (OOB) determines the model accuracy using generalization error estimation (Breiman 2001). Diversity among the classification trees increases using resampling the data with replacement and also randomly change of predictors set during tree induction processes (Youssef et al., 2016). Information from numerous decision trees has been combined in the RF algorithm.

Generally, it is essential to define two parameters to run the RF model including the number of trees (ntree) and the number of factors prepared from the data shown in Fig. 3 (mtry). The former is built while the RF model is running, while the latter is used in the tree-building process. Both the number of trees and factors need to be optimized to minimize the generalization error (Rahmati et al. 2016). The optimisation was done through sensitivity tests.

2.4.2 Artificial neural network (ANN)

The artificial neural network (ANN) is a machine learning tool developed by imitating human brain performances and making connections between inputs and outputs (Sakizadeh et al. 2017). The human brain is mimicked in two ways: Firstly, obtaining information and knowledge using a learning process, and secondly, storing knowledge using synaptic weights. Therefore, ANN has been identified as the model that finds the optimal solution for non-linear problems, such as dust source and soil erosion

susceptibility, by identifying patterns with conditioning factors (Ghorbanzadeh et al. 2019). In an ANN, a neuron is the smallest data processing unit which could make many neural network structures and be used in research for different purposes. The standard structure of ANN consists of three layers, namely, the input layer, the hidden layers, and the output layer. The input layer consists of training data and conditioning factors of dust source, the neurons in the hidden layer analyze the complex information contained in the data, and the output layer is the maps of dust source susceptibility. In this structure, the neurons across the same layer are not connected, but they are linked with neurons in the previous and subsequent layers. In ANN, the algorithm determines a weight for each input factor and a transfer function to build results (Kalantar et al. 2017).

2.4.3 Flexible discriminate analyses (FDA)

The modification of the linear regression model for the application to non-linear problems is the purpose of FDA (Avand et al. 2021). Nonparametric regression models, nonlinear discriminant analysis, and classification methods are combined into one framework. This algorithm is flexible for non-linear classifications because non-linear transformation is used and clusters are soft (Kalantar et al. 2020), here clusters for the relationship between soil erosion and the predictor factors from Fig. 3. In this way, variables in FDA are firstly aligned with the multivariate adaptive regression splines (MARS) and then dimension reduction is performed (Kim and Kim 2021). FDA can overcome the problem of linear discriminant analysis (LDA) and it is minimizing the square average of the residuals (Mosavi et al. 2020), while linear regression is replaced by nonparametric regression in FDA. Therefore, FDA has the potential to apply for non-linear natural problems such as soil erosion, dust, flood, and landslide.

2.5. Evaluation of machine learning algorithms

In our DSSA and SESA assessment, 70% of point data are randomly selected for the training dataset and 30% for model validation. The prediction accuracy of the machine learning algorithms is assessed by comparing the DSSA map with the validation dataset of dust sources. These data were extracted from MODIS images and some indicators which were explained in section 2.1.2. The Receiver Operating Characteristic (ROC) curve and the Area Under the Curve (AUC) are applied following past studies that used these to test the prediction skill of a model for the occurrence or non-occurrence of the

studied phenomena (Naghibi et al. 2017). The AUC ranges from 0 to 1 in which the models that better perform represent the AUC close to one.

3. Results and Discussion

3.1. Spatial distribution of DSSA

3.1.1. Dust aerosol detection

An illustration of a dust storm seen in MODIS FCC satellite imagery over the Lut watershed on August 7, 2019, is shown in Fig. 4. Following a visual analysis of the images, we determined that the false colour combination (R: BTD2931, G: Band 4, B: Band 3) is the best and applied it to 26 MODIS images of dusty days. As a result, the Lut watershed's dust source locations were identified (Fig. 4).

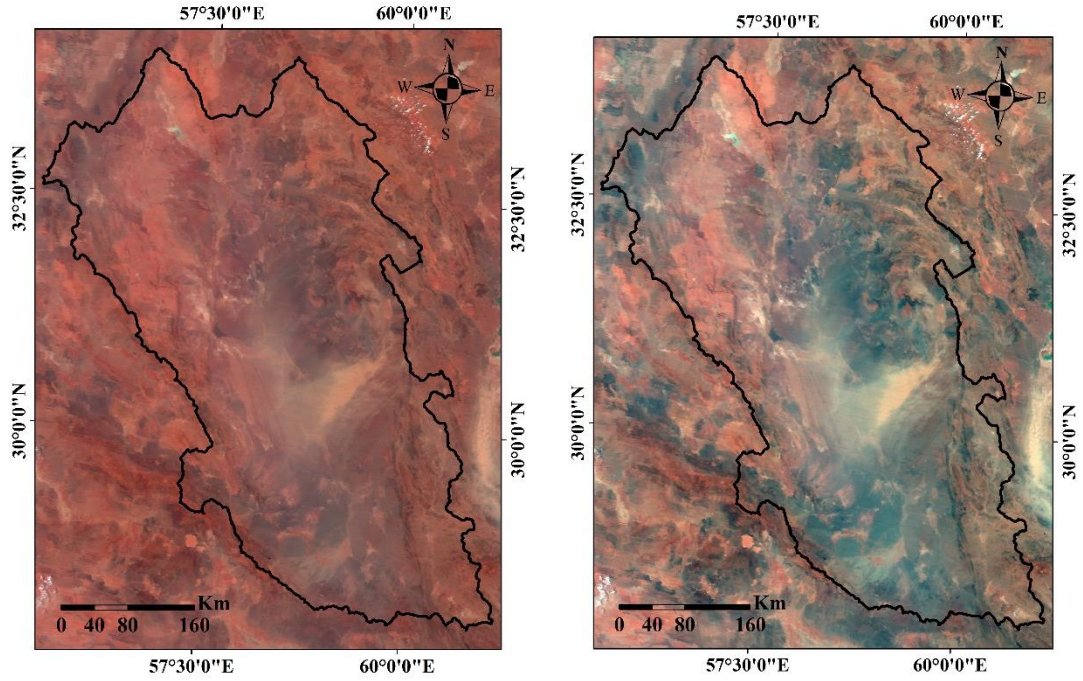

Fig.4 The dust storm on 07 August 2019, as seen above is an example of the visual inspection of a dust storm (a) MODIS true colour (Red: Band 5, Green: Band 4, Blue: Band 3), and (b) enhanced MODIS satellite photos, (Red: BTD2931, Green: Band 4, Blue: Band 3).

3.1.2 The importance of conditioning factors for DSSA

Since multicollinearity among factors has been identified as an obstacle to explaining the results (Roy and Saha 2019), the Variance Inflation Factor (VIF) was calculated to assess the relationships among conditioning factors. This was conducted because multicollinearity among factors will decline the accuracy of the models (Arabameri et al. 2019b). In the present study, VIF values for DSSA mapping range from 1.05 to 1.57 which illustrated no collinearity among the eight factors. Therefore, no exclusion was applied and all factors were considered in successor calculations and modeling.

The importance and impact of each factor depend on the machine learning algorithms. The result of DSSA mapping using RF showed that NDVI, elevation, land use, and lithology had the greatest degree of effect among conditioning factors. Land use and NDVI as an index of vegetation cover proved to have a controlling impact on wind erosion and dust emission (Gholami et al., 2020). Elevation is an effective factor for DSSA in which lowlands have higher impacts than highlands. This was confirmed by other studies such as Darvand et al., 2021. Lithology is another important factor in this watershed since dust emission is mostly occur in the sensitive lithology rather than resistant ones (Sissakian et al., 2013). Overall, the impacts of these factors on DSSA have been proved by previous investigations (Gholami et al. 2020a, 2020b). Other factors such as the distance from rivers, rainfall, and slope were identified as rather weak predictors, respectively. These findings agree with other research (Boroughani and Pourhashemi 2020, Darvand et al. 2021).

The FDA approach showed that however elevation, NDVI, and land use had the highest effects on dust sources susceptibility, other factors had no impact on DSSA. Similarly, with ANN, elevation, NDVI, and land use were identified as the three most effective factors, and other factors were weaker predictors rather than formers. However these two models of FDA and ANN provide similar results in term of the importance of conditioning factors, FDA could be used rather than ANN because of its higher accuracy which is shown in the next section.

3. 1. 3 Spatial distribution of dust source susceptibility

The dust source susceptibility (DSS) maps created by RF, FDA, and ANN are classified into five risk classes (very high, high, moderate, low, and very low) shown in Fig. 5. These classes are set as in earlier studies (Mosavi et al., 2020; Boroughani, Mohammadi, Mirchooli, & Fiedler, 2022). The results of the model evaluation using ROC indicates that the RF model with an accuracy of 75.0% provides the most accurate

outputs. FDA and ANN had similar performances with the accuracy of 71.7% and 70.7%. In terms of True Skill Statistic (TSS), similar results have been obtained in which RF with an accuracy of 45.8% had again the best performance in comparison to FDA (32.4%) and ANN (35.8%). In this way, RF introduces different priorities for the effective factors in comparison with FDA and ANN. RF proposes NDVI, elevation, land use, and lithology as the most important factors, while FDA and ANN suggest elevation, NDVI, and land use as the most influencing factors. The dominance of NDVI, elevation and land use as the most effective factors for DSS is consistent with the understanding of dust source locations that are typically found in topographic depressions with sparse or no vegetation. The DSSA map from RF was selected for further analysis due to the highest accuracy, although the differences between FDA and ANN are in the statistical sense relatively small. According to the DSSA maps, 29% and 17% of the watershed were classified as areas of high and very high DSSA, i.e., almost half of the study area. Only 4% and 16% of the watershed have a very low and low susceptibility to soil erosion through winds, respectively. The spatial extent of high and very high risk areas from RF is smaller than the ones obtained by ANN and FDA. In all three maps, it can be seen that the biggest potential for dust emission is located in the central parts (Lut Desert) of the watershed. These results are consistent with other research, indicating that RF allows more detailed spatial mapping of dust source susceptibility compared to other machine learning algorithms (Rahmati et al. 2020, Gholami et al. 2019b, Darvand et al. 2021).

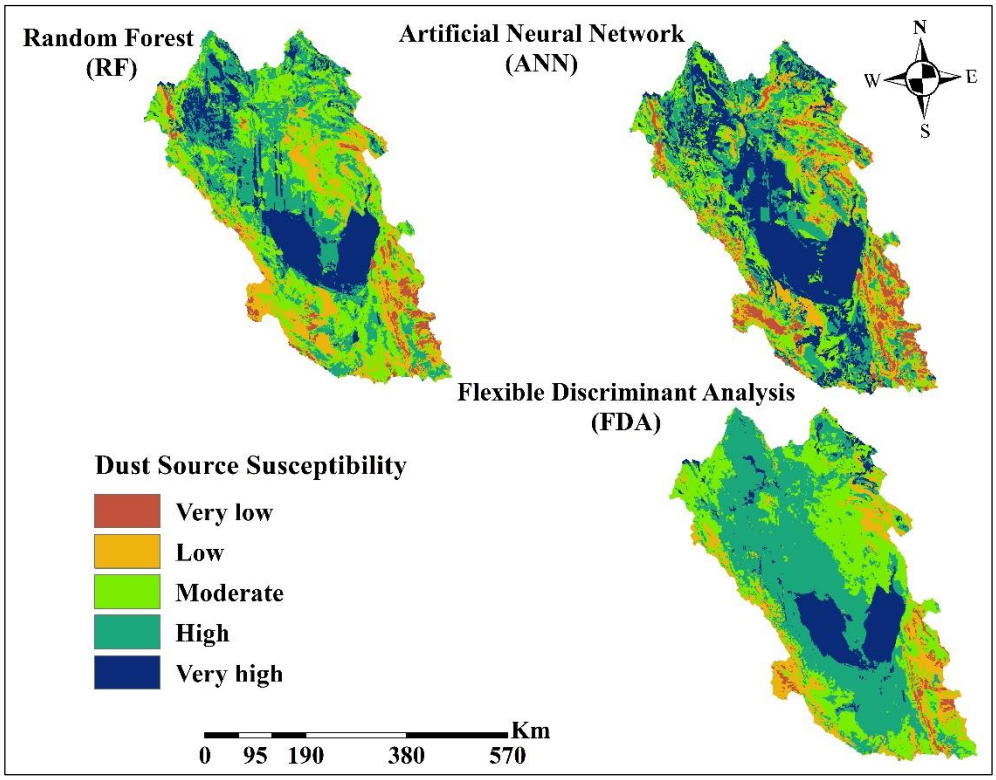

Fig. 5 Dust sources susceptibility area (DSSA) based on random forest (RF), artificial neural network (ANN), and flexible discriminate analyses (FDA)

As mentioned before, the watershed is one of the key regions with dust concentration in southwest Asia. Spatial distribution of dust sources in this region is a key roadmap for preventive and adaptive measurement. This would reduce dust emission across the watershed, region, and even other near countries.

3.2. Soil erosion susceptibility map

3.2.1 Relative influential conditioning factors for SESA

There are some differences in the contributions of influential factors among models. So that, RF indicates that rainfall, TWI, slope, elevation, land use, and geology are the most important conditioning factors. Considering this watershed located in arid region of Iran, rainfall and TWI play decisive and crucial role in soil erosion among them. TWI which indicate soil moisture and water-saturated area (Silva et al., 2023) has been also identified an effective factor for different kinds of soil erosion such as rill-interrill, gully, and piping erosions (Sholagberu et al., 2017; Hosseinalizadeh et al., 2019). Slope influences also soil erosion rate through effecting on runoff velocity, vegetation cover, and soil type (Avand et al., 2022). This conditioning factor has been also reported as

one of the most influential factor in most studies (Sholagberu et al., 2017; Pournader et al., 2018; Lei et al., 2020). Moreover, distance from roads and rivers were recognized as the least important factors. These findings of the impact of conditioning factors for SESA are similar in other regions (Arabameri et al. 2019a, Hosseinalizadeh et al. 2019). For ANN, TWI, slope, and land use were the most effective factors for prediction which is followed by NDVI, land use, and distance from the river. The results from FDA indicated that the most important conditioning factors are TWI, slope, and elevation, geology, and NDVI. TWI has an important impact on SESA in all three models. This is because the study watershed predominates with low slopes and elevations. The opposite result of this finding was obtained by Silva et al., 2023.

A large area of the watershed is land with typically little rain and vegetation cover such that bare soil is the main physical attribute in the watershed. This kind of surface is known to be prone to water-induced soil erosion, when rain events occur. The erosion can be particularly pronounced over slopes. This understanding is consistent with all algorithms pointing to a major role of TWI and slope for SESA.

Some environmental factors (rainfall, TWI, slope, elevation, and geology) influence SESA more than DSSA. Land use as a human-induced conditioning factor, however, affects both SESA and DSSA, which underlines the importance of land-use planning and management.

3.2.2. Spatial modeling of SESA

Fig. 6 shows the SESA predictions from the three machine learning algorithms, classified by the soil erosion risk in the ArcGIS environment. Validation of the three machine learning algorithms highlights that RF was again the most reliable algorithm amongst the three, indicated by the best prediction rate. Based on ROC, RF yields a 94% accuracy for SESA (Fig. 6c). The ROC coefficient of ANN and FDA were slightly lower, but still high with an accuracy of 91% and 89%, respectively. In the case of the TSS index, better performance was obtained again for RF (89%) rather than ANN (78%) and FDA (78%). High performance of RF model in classification issues is related to its potential to handle bigh datasets and apply large number of conditioning factors (Naghibi et al., 2018). In addition, Rahmati et al., 2020 states that high accuracy of RF is the results of several advantage of this model such as iterative nature and preventing problems by overfitting (Rahmati et al., 2020).

The majority of the land in the watershed (81%) has a high and very high risk for water-induced soil erosion by RF. This is slightly lower than for ANN and FDA which classified 85% and 89% of the watershed as high and very high susceptible areas. The high and very high susceptible areas for water-driven soil erosion are mostly located in the north and south-west parts of the watershed. The high and very high susceptible areas have socio-economic implications, particularly because most settlements and cities of the watershed are located in the same regions. This can mean that human activity is a contributing factor to the water-induced soil erosion. Mutually, intensified soil erosion might lead to migration of resident people to other places and even other countries.

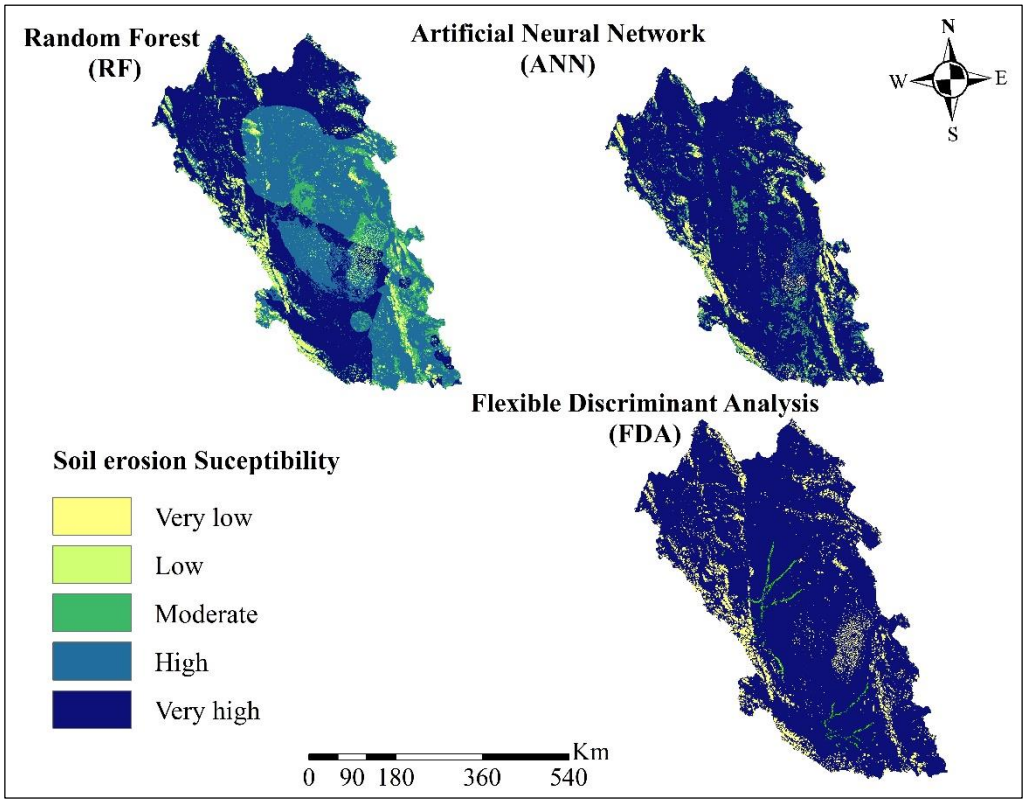

Fig. 6 soil erosion susceptibility areas map (GESM) using random forest (RF), artificial neural network (ANN), and flexible discriminate analyses (FDA)

3.3. Land degradation susceptibility

The majority of the study watershed is susceptible to a substantial risk for land degradation. The spatial distribution of land degradation susceptibility, shown in Fig. 7, indicates that only 4% of the land area has low to very low risks of land degradation. Areas susceptible to both soil erosion by water and winds together constitute 43% of

the total area. Approximately 45% and 8% of the study area are at risk of soil erosion by water and wind, respectively. Taken together, it means that the majority of the Lut watershed falls under the category of land degradation risks. The watershed accounts for 12.5% of the total land of Iran. The findings of the present study are therefore consistent with a report that indicated water erosion as an environmental hazard in Iran (Bui et al. 2019). The results of the study will be helpful and applicable for identifying water-induced and dust sources hotspots across the watershed and prioritizing appropriate conservation measurements and rehabilitative policies.

The areas that fall under the category of both kind of land degradation might be most vulnerable concerning local self-sufficiency for food security and sustainability of human activities. For instance, dust storms drive water loss through failure of agricultural crops in Iran (Boroughani et al. 2022). Moreover, the adverse impacts of water-induced soil erosion are known from numerous other regions (Lal and Moldenhauer 2008, Gao et al. 2015, Standardi et al. 2018; Roy et al., 2022).

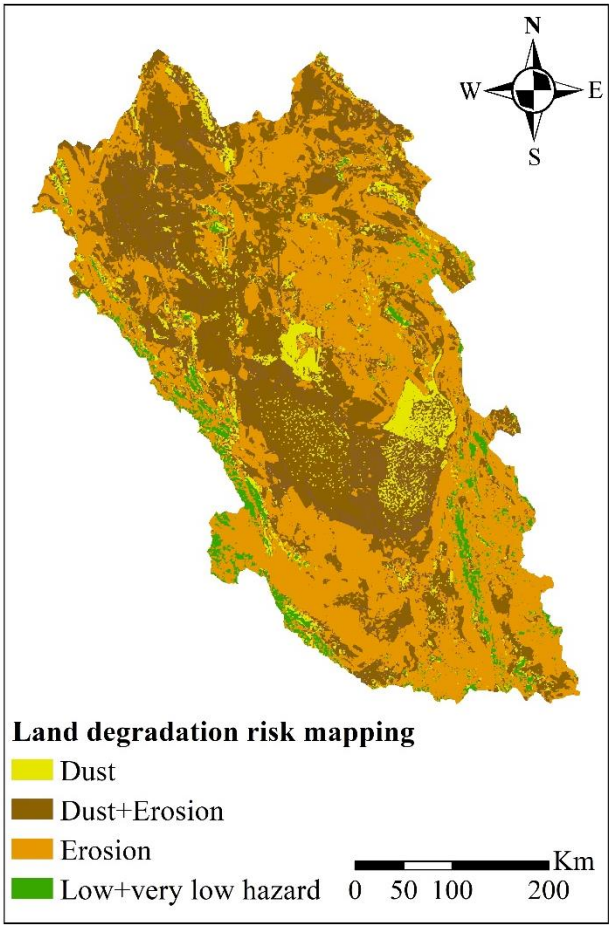

Fig. 7 Land degradation susceptibility map in terms of soil erosion and dust sources areas

Conclusion

Investigation of soil erosion through water along with wind-driven soil erosion from dust sources have received little attention in past studies, despite their importance for land degradation with associated social, economic, and environmental impacts. The present study used several different data sets, conducted a field survey and paired the data with three different machine learning algorithms to construct spatial maps for areas of risk for land degradation for the Lut watershed in Iran. Three machine learning algorithms were successfully applied to create land susceptibility maps describing dust aerosol occurrence considering methodological uncertainty. In addition, these models were used to identify the areas prone to soil erosion by surface water runoff. These obtained maps were synthesized to generate a single map for risks of land degradation. The results of the present study show that the random forest algorithm outperformed the other two machine learning approaches for both dust sources and soil erosion susceptibility mapping with an accuracy of 75% and 94%, respectively.

As expected, the vegetation cover, elevation, land use, and geology were important prerequisites for dust-emission occurrence in the watershed, while rainfall, Topographical Wetness Index (TWI), terrain slope, terrain elevation, land use, and geology were identified as the most influential factors for water-induced soil erosion.

Based on the land degradation map, almost the entire study region is at risk. A large fraction of 43% of the area is prone to both high wind-driven plus water-driven soil erosion. In addition to these areas, another 45% and 8% of the area have a risk for water-driven and wind-driven soil erosion, respectively. The methods tested in this study could be later transferred to similar assessments in other regions around the world. Choosing this region in Iran is further motivated by the impact of land degradation on the country's economy. The current study has some limitation including the small sample size and non-uniform distribution of water-induced soil erosion points because of lack of accessibility to a road network in some parts of the watershed. Despite these limitations, these results can potentially be useful for managers and policy makers to identify local hotspots for land degradation to implement mitigation and adaptation measures in this watershed. Future studies could work on improving the spatial resolution and coverage of the risk assessment for providing more information on risks for land degradation. In addition, it is suggested that future research should estimate the role of other climatic factors such as humidity, and air temperature on soil erosion and dust source susceptibility. Prediction of NDVI and rainfall as the most effective factors

on soil erosion and dust sources and estimated of their impacts on future water induced-soil erosion and dust sources susceptibility is also suggested for the other studies. It requires more measurements for soil erosion by water and winds to train the machine learning models.

Acknowledgement

SF acknowledges funding from the German Research Foundation (DFG) for SFB 1502/1–2022 (Project: 450058266).

Conflict of Interest

The authors declare that there is no conflict of interests regarding the publication of this article.

References

Amiri M, Pourghasemi HR, Ghanbarian GA, Afzali SF (2019) Assessment of the importance of gully erosion effective factors using Boruta algorithm and its spatial modeling and mapping using three machine learning algorithms. Geoderma 340:55–69. https://doi.org/10.1016/j.geoderma.2018.12.042

Anache JAA, Flanagan DC, Srivastava A, Wendland EC (2018) Land use and climate change impacts on runoff and soil erosion at the hillslope scale in the Brazilian Cerrado. Science of the Total Environment 622–623:140–151. https://doi.org/10.1016/j.scitotenv.2017.11.257

Arabameri A, Chen W, Loche M, et al (2019a) Comparison of machine learning models for gully erosion susceptibility mapping. Geoscience Frontiers. https://doi.org/10.1016/j.gsf.2019.11.009

Arabameri A, Pradhan B, Rezaei K (2019b) Gully erosion zonation mapping using integrated geographically weighted regression with certainty factor and random forest models in GIS. Journal of Environmental Management 232:928–942. https://doi.org/10.1016/j.jenvman.2018.11.110

Avand M, Moradi HR, Lasboyee MR (2021) Spatial prediction of future flood risk: An approach to the effects of climate change. Geosciences (Switzerland) 11:1–20. https://doi.org/10.3390/geosciences11010025

Beven KJ, Kirkby MJ (1979) A physically based, variable contributing area model of basin hydrology/Un modèle à base physique de zone d'appel variable de l'hydrologie du bassin versant. Hydrological sciences journal 24:43–69

Boroughani M, Mohammadi M, Mirchooli F, Fiedler S (2022) Assessment of the impact of dust aerosols on crop and water loss in the Great Salt Desert in Iran. Computers and Electronics

in Agriculture 192:106605

Boroughani, M., Pourhashemi, S., Gholami, H., & Kaskaoutis, D. G. 2021. Predicting of dust storm source by combining remote sensing, statistic-based predictive models and game theory in the Sistan watershed, southwestern Asia. Journal of Arid Land, 13(11), 1103-1121.

Boroughani M, Pourhashemi S (2020) Susceptibility Zoning of Dust Source Areas by Data Mining Methods over Khorasan Razavi Province. Quarterly journal of Environmental Erosion Research 9:1–22

Boroughani M, Pourhashemi S, Hashemi H, et al (2020) Application of remote sensing techniques and machine learning algorithms in dust source detection and dust source susceptibility mapping. Ecological Informatics 56:101059. https://doi.org/10.1016/j.ecoinf.2020.101059

Breiman L (2001) Random forests. Machine Learning 45:5–32. https://doi.org/10.1023/A:1010933404324

Bui DT, Shirzadi A, Shahabi H, et al (2019) A novel ensemble artificial intelligence approach for gully erosion mapping in a semi-arid watershed (Iran). Sensors (Switzerland) 19:. https://doi.org/10.3390/s19112444

Chicas SD, Omine K, Ford JB (2016) Identifying erosion hotspots and assessing communities ' perspectives on the drivers , underlying causes and impacts of soil erosion in Toledo 's Rio Grande Watershed : Belize. Applied Geography 68:57–67. https://doi.org/10.1016/j.apgeog.2015.11.010

Darvand S, Khosravi H, Keshtkar H, et al (2021) Comparison of machine learning models to prioritize susceptible areas to dust production. Journal of Range and Watershed Managment 74:53–68

Derakhshan-Babaei F, Mirchooli F, Mohammadi M, et al (2022) Tracking the origin of trace metals in a watershed by identifying fingerprints of soils, landscape and river sediments. Science of The Total Environment 155583

Ebrahimi-khusfi Z, Taghizadeh-mehrjardi R, Mirakbari M (2021) Evaluation of machine learning models for predicting the temporal variations of dust storm index in arid regions of Iran. Atmospheric Pollution Research 12:134–147. https://doi.org/10.1016/j.apr.2020.08.029

Emadodin I, Narita D, Rudolf H (2012) Soil degradation and agricultural sustainability : an overview from Iran. Environment, Development and Sustainability 14:611–625. https://doi.org/10.1007/s10668-012-9351-y

Gao L, Bowker MA, Xu M, et al (2017) Biological soil crusts decrease erodibility by modifying inherent soil properties on the Loess Plateau, China. Soil Biology and Biochemistry 105:49–58. https://doi.org/10.1016/j.soilbio.2016.11.009

Gao X, Xie Y, Liu G, et al (2015) Effects of soil erosion on soybean yield as estimated by simulating gradually eroded soil profiles. Soil and Tillage Research 145:126–134

Garosi Y, Sheklabadi M, Conoscenti C, et al (2019) Assessing the performance of GIS- based machine learning models with different accuracy measures for determining susceptibility to gully erosion. Science of the Total Environment 664:1117–1132. https://doi.org/10.1016/j.scitotenv.2019.02.093

Gholami H, Kordestani MD, Li J, et al (2019a) Diverse sources of aeolian sediment revealed in an arid landscape in southeastern Iran using a modified Bayesian un-mixing model. Aeolian Research 41:100547

Gholami H, Mohamadifar A, Sorooshian A, Jansen JD (2020a) Machine-learning algorithms for predicting land susceptibility to dust emissions : The case of the Jazmurian Basin , Iran. Atmospheric Pollution Research 11:1303–1315. https://doi.org/10.1016/j.apr.2020.05.009

Gholami H, Mohammadifar A, Collins AL (2019b) Spatial mapping of the provenance of storm dust: Application of data mining and ensemble modelling Hamid. Atmospheric Research 104716. https://doi.org/10.1016/j.atmosres.2019.104716

Gholami H, Mohammadifar A, Pourghasemi HR, Collins AL (2020b) A new integrated data mining model to map spatial variation in the susceptibility of land to act as a source of aeolian dust. Environmental Science and Pollution Research 27:42022–42039

Ghorbanzadeh O, Kamran KV, Blaschke T, et al (2019) Spatial Prediction of Wildfire Susceptibility Using Field Survey GPS Data and Machine Learning Approaches. fire 2:1–23

Gia T, Degener J, Kappas M (2018) Integrated universal soil loss equation (USLE) and Geographical Information System (GIS) for soil erosion estimation in A Sap basin : Central Vietnam. International Soil and Water Conservation Research 6:99–110. https://doi.org/10.1016/j.iswcr.2018.01.001

Halecki W, Kruk E, Ryczek M (2018) Land Use Policy Loss of topsoil and soil erosion by water in agricultural areas : A multi- criteria approach for various land use scenarios in the Western Carpathians using a SWAT model. Land Use Policy 73:363–372. https://doi.org/10.1016/j.landusepol.2018.01.041

Hosseinalizadeh M, Kariminejad N, Rahmati O, et al (2019) How can statistical and artificial intelligence approaches predict piping erosion susceptibility? Science of the Total Environment 646:1554–1566. https://doi.org/10.1016/j.scitotenv.2018.07.396

Hahnenberger, M., Nicoll, K., 2014. Geomorphic and land cover identification of dust sources in the eastern Great Basin of Utah, U.S.A. Geomorphology 204 (2), 657–672. https://doi.org/10.1016/j.geomorph.2013.09.013.

Jafari M, Mesbahzadeh T, Masoudi R, et al (2021) Dust storm surveying and detection using remote sensing data, wind tracing, and atmospheric thermodynamic conditions (case study: Isfahan Province, Iran). Air Quality, Atmosphere & Health 1–11

٦٣٩ Kalantar B, Pradhan B, Naghibi SA, et al (2017) Assessment of the effects of training data
٦٤٠ selection on the landslide susceptibility mapping: a comparison between support vector
٦٤١ machine (SVM), logistic regression (LR) and artificial neural networks (ANN). Geomatics,
٦٤٢ Natural Hazards and Risk 5705:1–21. https://doi.org/10.1080/19475705.2017.1407368
٦٤٣ Kalantar B, Ueda N, Saeidi V, et al (2020) Landslide susceptibility mapping: Machine and
٦٤٤ ensemble learning based on remote sensing big data. Remote Sensing 12:1–23.
٦٤٥ https://doi.org/10.3390/rs12111737
٦٤٦ Kim JW, Kim HG (2021) Landslide susceptibility analysis by type of cultural heritage site
٦٤٧ using ensemble model: Case study of the Chungcheong Region of South Korea. Sensors and
٦٤٨ Materials 33:3819–3833. https://doi.org/10.18494/SAM.2021.3593
٦٤٩ Lal R, Moldenhauer WC (2008) Effects of soil erosion on crop productivity. Effects of soil
٦٥٠ erosion on crop productivity 5:303–367. https://doi.org/10.1080/07352688709382244
٦٥١ Lee S, Hong S-M, Jung H-S (2017) GIS-based groundwater potential mapping using artificial
٦٥٢ neural network and support vector machine models: the case of Boryeong city in Korea.
٦٥٣ Geocarto International 6049:1–15. https://doi.org/10.1080/10106049.2017.1303091
٦٥٤ Lee, J. A., Gill, T. E., Mulligan, K. R., Acosta, M. D., Perez, A. E. 2009. Land use/land cover
٦٥٥ and point sources of the 15 December 2003 dust storm in southwestern North
٦٥٦ America. Geomorphology, 105(1-2), 18-27
٦٥٧ Mirchooli F, Motevalli A, Pourghasemi HR, et al (2019) How do data-mining models consider
٦٥٨ arsenic contamination in sediments and variables importance? Environmental Monitoring and
٦٥٩ Assessment 191:. https://doi.org/10.1007/s10661-019-7979-x
٦٦٠ Mosavi A, Golshan M, Janizadeh S, et al (2020) Ensemble models of GLM, FDA, MARS, and
٦٦١ RF for flood and erosion susceptibility mapping: a priority assessment of sub-basins. Geocarto
٦٦٢ International. https://doi.org/10.1080/10106049.2020.1829101
٦٦٣ Naghibi SA, Ahmadi K, Daneshi A (2017) Application of Support Vector Machine, Random
٦٦٤ Forest, and Genetic Algorithm Optimized Random Forest Models in Groundwater Potential
٦٦٥ Mapping. Water Resources Management 31:2761–2775. https://doi.org/10.1007/s11269-017-
٦٦٦ 1660-3
٦٦٧ Park S, Kim J, Lee J, et al (2014) Combined dust detection algorithm by using MODIS infrared
٦٦٨ channels over East Asia. Remote Sensing of Environment 141:24–39.
٦٦٩ https://doi.org/10.1016/j.rse.2013.09.019
٦٧٠ Péré J-C, Rivellini L, Crumeyrolle S, et al (2018) Simulation of African dust properties and
٦٧١ radiative effects during the 2015 SHADOW campaign in Senegal. Atmospheric Research
٦٧٢ 199:14–28
٦٧٣ Rahmati O, Mohammadi F, Saeid S, et al (2020) Identifying sources of dust aerosol using a
٦٧٤ new framework based on remote sensing and modelling. Science of the Total Environment
٦٧٥ 737:139508. https://doi.org/10.1016/j.scitotenv.2020.139508

٦٧٦ Rahmati O, Pourghasemi HR, Melesse AM (2016) Application of GIS-based data driven
٦٧٧ random forest and maximum entropy models for groundwater potential mapping: A case study
٦٧٨ at Mehran Region, Iran. Catena 137:360–372. https://doi.org/10.1016/j.catena.2015.10.010
٦٧٩ Roy J, Saha S (2019) GIS-based Gully Erosion Susceptibility Evaluation Using Frequency
٦٨٠ Ratio , Cosine Amplitude and Logistic Regression Ensembled with fuzzy logic in Hinglo River
٦٨١ Basin , India. Remote Sensing Applications: Society and Environment 15:100247.
٦٨٢ https://doi.org/10.1016/j.rsase.2019.100247
٦٨٣ Sakizadeh M, Mirzaei R, Ghorbani H (2017) Support vector machine and artificial neural
٦٨٤ network to model soil pollution : a case study in Semnan Province , Iran. Neural Computing
٦٨٥ and Applications 28:3229–3238. https://doi.org/10.1007/s00521-016-2231-x
٦٨٦ Shi P, Yan P, Yuan Y, Nearing MA (2004) Wind erosion research in China: Past, present and
٦٨٧ future. Progress in Physical Geography 28:366–386.
٦٨٨ https://doi.org/10.1191/0309133304pp416ra
٦٨٩ Shit PK, Pourghasemi H reza, Bhunia GS (2020) Gully Erosion Studies from India and
٦٩٠ Surrounding Regions
٦٩١ Standardi G, Panagos P, Montanarella L, et al (2018) Cost of agricultural productivity loss due
٦٩٢ to soil erosion in the European Union : From direct cost evaluation approaches to the use of
٦٩٣ macroeconomic models. Land Degradation & Development 29:471–484.
٦٩٤ https://doi.org/10.1002/ldr.2879
٦٩٥ Sun W, Shao Q, Liu J, Zhai J (2014) Assessing the effects of land use and topography on soil
٦٩٦ erosion on the Loess Plateau in China. Catena 121:151–163.
٦٩٧ https://doi.org/10.1016/j.catena.2014.05.009
٦٩٨ Tehrany MS, Pradhan B, Jebur MN (2014) Flood susceptibility mapping using a novel
٦٩٩ ensemble weights-of-evidence and support vector machine models in GIS. Journal of
٧٠٠ Hydrology 512:332–343. https://doi.org/10.1016/j.jhydrol.2014.03.008
٧٠١ Yang M, Zhu X, Pan H, et al (2019) Changes of the relationship between spring sand dust
٧٠٢ frequency and large-scale atmospheric circulation. Atmospheric Research 226:102–109.
٧٠٣ https://doi.org/10.1016/j.atmosres.2019.04.004
٧٠٤ Youssef AM, Pourghasemi HR (2021) Landslide susceptibility mapping using machine
٧٠٥ learning algorithms and comparison of their performance at Abha Basin, Asir Region, Saudi
٧٠٦ Arabia. Geoscience Frontiers 12:639–655
٧٠٧ Zabihi M, Mirchooli F, Motevalli A, et al (2018) Spatial modelling of gully erosion in
٧٠٨ Mazandaran Province, northern Iran. Catena 161:1–13.
٧٠٩ https://doi.org/10.1016/j.catena.2017.10.010
٧١٠ Zerihun M, Mohammedyasin MS, Sewnet D, et al (2018) Assessment of soil erosion using
٧١١ RUSLE, GIS and remote sensing in NW Ethiopia. Geoderma Regional 12:83–90.
٧١٢ https://doi.org/10.1016/j.geodrs.2018.01.002

٧١٣ Vickery, K., Eckardt, F. 2013. Dust emission controls on the lower Kuiseb River valley, central
٧١٤ Namib. Aeolian Res. 10, 125–133. https://doi.org/10.1016/j.aeolia.2013.02.006.
٧١٥ Walker, A.L., Liu, M., Miller, S.D., Richardson, K.A., Westphal, D.L., 2009. Development of
٧١٦ a dust source database for mesoscale forecasting in Southwest Asia. J. Geophys. Res. 114 (18),
٧١٧ 1–24. https://doi.org/10.1029/2008JD011541.